

Interlook Cross-Correlation Function of Speckle in SAR Images of Sea Surface Processed With Partially Overlapped Subapertures

Kazuo Ouchi, *Senior Member, IEEE*, and Haipeng Wang, *Student Member, IEEE*

Abstract—In the present paper, a general integral expression is derived and discussed for the cross-correlation function (CCF) of speckle patterns in synthetic aperture radar (SAR) images processed by using partially overlapped subapertures of arbitrary Doppler center frequencies (or equivalent azimuth times). It is shown that, under the white noise approximation for the backscattered field, the CCF of the interlook speckle intensity patterns is given by the squared modulus of the autocorrelation function of the amplitude weighting function of subapertures where the time lag is the center time difference. It is also shown that the CCF of the interlook speckle patterns is independent of the surface coherence time of sea surface. The integral expression for the intensity CCF is then evaluated for a rectangular weighting function, and comparison is made with Japanese Earth Resources Satellite-1 (JERS-1) L-band and RADARSAT-1 C-band SAR images of sea surface to test the theory. The CCFs computed from the JERS-1 SAR data show excellent agreement with the theory, and good agreement is obtained with the RADARSAT-1 data.

Index Terms—Cross-correlation function (CCF), scene coherence time, sea surface, speckle, synthetic aperture radar (SAR).

I. INTRODUCTION

MULTILOOK processing is a well-known technique of speckle noise reduction and simultaneous equalization of two-dimensional resolution scale in synthetic aperture radar (SAR) imagery. It is based on incoherent addition of uncorrelated multilook intensity images produced with nonoverlapping subapertures (an equivalent result, for stationary surfaces, can be obtained by averaging neighboring pixels in the full single-look intensity images), and a substantial number of publications concerning this issue are available (e.g., [1]–[4]). However, it is surprising to find that very little, to the authors' knowledge, is reported in open literature on the interlook cross-correlation property between speckle patterns produced by using partially overlapped subapertures. An exception is the theoretical study of Ouchi and Burge [5] who describe the cross-correlation function (CCF) for Gaussian amplitude subaperture weightings. Their results also show that the CCF is independent of a scene coherence time of randomly fluctuating sea surfaces, provided that the backscattered field is modeled as a Gaussian white noise. However, no experimental data were provided to support the theory. In the recent paper [6] of ship detection

by the cross-correlation technique, it is experimentally shown that the interlook cross-correlation function of speckle intensity in the RADARSAT-1 images of sea surface produced by partially overlapped subapertures appears to be independent of the scene coherence time.

Thus, the purpose of this paper is to report the theoretical study on the cross-correlation function of intensity speckle patterns in terms of the center time difference of partially overlapped subapertures, and the experimental results using real SAR data for comparison with the theory. In the first part of the paper, a general integral expression for the intensity CCF of speckle patterns produced through partially overlapped subapertures at arbitrary center times is derived and discussed. An assumption is made that the backscattered spatial field is modeled as being statistically “white,” so that the resultant speckle patterns between subimages produced by nonoverlapping subapertures are spatially uncorrelated. Further, the theory takes account of the random temporal fluctuation of the return signal from the sea surface. The result shows that the interlook speckle CCF is proportional to the modulus square of the autocorrelation function of the subaperture amplitude weighting function, where the time lag variable is the center time difference. It is also shown that the interlook speckle CCF is independent of the temporal fade process of the backscattered field. For simplicity, the theoretical treatment is given only in the azimuth direction, since the multilook processing is applied to the azimuth component. An analytic expression of the interlook CCF is then derived from the integral equation for a rectangular amplitude weighting of subapertures. Finally, this theoretical CCF is compared with those computed from the Japanese Earth Resources Satellite-1 (JERS-1) L-band SAR and RADARSAT-1 C-band SAR images over the coastal waters of Japan.

II. BASIC THEORY

A. Siegert Relation

When a statistically homogeneous random rough surface is imaged by a SAR, a Gaussian speckle pattern, inherent to coherent systems, is formed. The term “Gaussian” stems from the fact that the real and imaginary parts of the complex amplitude of the speckle field obey a Gaussian probability density function (pdf), provided that more than about four to eight independent scatterers exist within a resolution cell to satisfy the central limit theorem [7], [8]. It is well known that the amplitude and intensity fluctuations of such speckle patterns are described by the

Manuscript received June 10, 2004; revised October 1, 2004.

The authors are with the Department of Environmental Systems Engineering, Kochi University of Technology, Kochi 782-8502, Japan (e-mail: ouchi.kazuo@kochi-tech.ac.jp).

Digital Object Identifier 10.1109/TGRS.2004.842439

Rayleigh and negative exponential pdfs, respectively [1]–[3]. It is also well known that the intensity CCF of Gaussian speckle patterns in the subimages can be described by the Siegert coherence function [3], [9]

$$\langle I(X; T_n)I(X; T_{n'}) \rangle = \langle I \rangle^2 + |\langle A(X; T_n)A^*(X; T_{n'}) \rangle|^2 \quad (1)$$

where the angular brackets indicate taking an ensemble average (expectation value), $I(X; T_n)$ is the intensity at an image position X produced by the subaperture of center time T_n , A is the image complex amplitude, and the asterisk $*$ means taking complex conjugate. The relation of (1) is valid if the random fluctuation in the image is a wide-sense stationary Gaussian process with $\langle I(X; T_n) \rangle = \langle I(X; T_{n'}) \rangle$. Equation (1) shows that the intensity CCF is proportional to the modulus square of the autocorrelation function of speckle amplitude.

B. Image Complex Amplitude of Arbitrary Center Time

In order to evaluate (1), the expression for the image complex amplitude $A(X; T_n)$ needs to be derived by taking into account the random temporal fluctuation of the scattering surface. It is important, therefore, to start the analysis from the SAR image formation with an arbitrary azimuth center time as follows.

A SAR antenna transmits a series of pulses and receives return signals as it propagates in the azimuth direction. A signal received at an azimuth time t from a point scatterer at an azimuth surface position x is given by

$$E_s(x, t) = a_s(x)a_t(t|x) \exp(-i2kr(x, t)) \quad (2)$$

where $k = 2\pi/\lambda$ is the wavenumber, λ is the wavelength, and $r(x, t)$ is the distance between the radar and the scatterer. The scattering amplitude is factorized to the spatial field $a_s(x)$ and its temporal change $a_t(t|x)$, where the temporal change is conditional upon the scatterer being observed at x , and it is a function of the azimuth time t only [10]. Examples corresponding to this type of scattering objects include the sea surface that is the subject of the present study, and forests on land under strong wind conditions.

It should be noted that, in practice, the amplitude of the return signal of (2) is weighted by the illuminating azimuth beam pattern. This weighting is removed in (2), because in the SAR processor used for the study [11] the beam pattern is corrected during the image forming process. The detailed explanation of the processor algorithm is beyond the scope of the present paper. However, in brief, the azimuth power spectrum is estimated first, and the amplitude of the image complex spectrum is smoothed before taking inverse fast Fourier transform to produce each look image. The Doppler offset varies with range, so that the smoothing is required for each azimuth line at different range positions.

The slant-range distance r can be approximated as follows:

$$\begin{aligned} r(x, t) &= \sqrt{R^2 + (Vt - x)^2} \\ &\simeq R + \frac{(Vt - x)^2}{2R}. \end{aligned} \quad (3)$$

In the expression, R is the slant-range distance when the radar is directly above (abeam of) the scatterer, and V is the platform

velocity. The return signal from an extended surface can then be given by substituting (3) into (2), and integrating the return signal of (2) over the surface with respect to the azimuth spatial variable x as

$$E(t) = E_0 \int_{-\infty}^{\infty} a_s(x)a_t(t|x) \exp\left(-i\frac{kV^2}{R}\left(t - \frac{x}{V}\right)^2\right) dx \quad (4)$$

where the term $\exp(-i2kR)$ has been absorbed in the constant E_0 . The complex amplitude of a look n image can be produced by correlating the return signal of (4) with a subreference signal E_r as

$$A(X; T_n) = \int_{-\infty}^{\infty} E\left(\frac{X}{V} + t\right) E_r(t) dt \quad (5)$$

where the look n subreference signal is given by

$$E_r(t; T_n) = W\left(\frac{t - T_n}{T}\right) \exp\left(i\frac{kV^2}{R}t^2\right) dt. \quad (6)$$

In this expression, W is the amplitude weighting function centered at the azimuth time T_n , and T is the integration time to synthesize the subaperture. Substituting (4) and (6) into (5) yields the complex amplitude of the look n image

$$\begin{aligned} A(X; T_n) &= A_0 \int_{-\infty}^{\infty} dx \int_{-\infty}^{\infty} dt W\left(\frac{t - T_n}{T}\right) a_s(x) \\ &\quad \cdot a_t\left(\frac{X}{V} + t|x\right) \exp\left(-i\frac{k}{R}(X - x)^2\right) \\ &\quad \cdot \exp\left(-i\frac{2kV}{R}(X - x)t\right) \end{aligned} \quad (7)$$

where A_0 is a normalizing constant.

C. General Integral Expression for CCF of Speckle Intensity

From (7), the amplitude CCF between the look n and look n' images can be expressed as

$$\begin{aligned} &\langle A(X; T_n)A^*(X; T_{n'}) \rangle \\ &= |A_0|^2 \int \int_{-\infty}^{\infty} dx_1 dx_2 \int \int_{-\infty}^{\infty} dt_1 dt_2 \\ &\quad \cdot W\left(\frac{t_1 - T_n}{T}\right) W^*\left(\frac{t_2 - T_{n'}}{T}\right) \\ &\quad \cdot \langle a_s(x_1)a_s^*(x_2) \rangle \\ &\quad \cdot \left\langle a_t\left(\frac{X}{V} + t_1|x_1\right) a_t^*\left(\frac{X}{V} - t_2|x_2\right) \right\rangle \\ &\quad \cdot \exp\left(-i\frac{k}{R}\left((X - x_1)^2 - (X - x_2)^2\right)\right) \\ &\quad \cdot \exp\left(-i\frac{2kV}{R}\left((X - x_1)t_1 - (X - x_2)t_2\right)\right). \end{aligned} \quad (8)$$

In order to simplify the four-fold integral of (8), the backscattered field is modeled as being statistically white. This assumption of a white noise approximation implies that the phases are random and distributed uniformly over $[0, 2\pi)$, and that they are

uncorrelated to each other and to the amplitudes [1]. The autocorrelation function of the backscattered spatial field can then be approximated by the following ensemble average:

$$\langle a_s(x_1)a_s^*(x_2) \rangle = \langle \sigma \rangle \delta(x_1 - x_2) \quad (9)$$

where $\langle \sigma \rangle$ is the radar cross section, and δ is the Dirac delta function. The temporal correlation function can be defined as [10]

$$\langle a_t(t_1|x_1)a_t^*(t_2|x_2) \rangle = \gamma(t_1 - t_2)|_{x_1=x_2} \quad (10)$$

which is a function of time difference between t_1 and t_2 only at a same surface position $x_1 = x_2$. In (9) and (10), the spatial and temporal fluctuations a_s and a_t are wide-sense stationary stochastic processes. Substituting (9) and (10) into (8), and integrating with respect to x_1 , (8) can be simplified to

$$\begin{aligned} \langle A(X; T_n)A^*(X; T_{n'}) \rangle &= |A_0|^2 \langle \sigma \rangle \int_{-\infty}^{\infty} dx \int_{-\infty}^{\infty} dt_1 dt_2 \\ &\cdot W\left(\frac{t_1 - T_n}{T}\right) W^*\left(\frac{t_2 - T_{n'}}{T}\right) \\ &\cdot \gamma(t_1 - t_2) \\ &\cdot \exp\left(-i\frac{2kV}{R}(X - x)(t_1 - t_2)\right) \end{aligned} \quad (11)$$

where $x = x_2$. The spatial extent of the statistically homogeneous surface is assumed to be large, then the integration of (11) with respect to x can be approximated as

$$\int_{-\infty}^{\infty} \exp\left(i\frac{2kV}{R}(t_1 - t_2)x\right) dx \simeq c_0 \delta(t_1 - t_2) \quad (12)$$

where c_0 is a constant with an appropriate dimension. Then, integrating (11) with respect to t_1 and putting $t = t_2$, (11) reduces to the following simple integral:

$$\begin{aligned} \langle A(X; T_n)A^*(X; T_{n'}) \rangle \\ = |A_0|^2 \int_{-\infty}^{\infty} W\left(\frac{t - T_n}{T}\right) W^*\left(\frac{t - T_{n'}}{T}\right) dt \end{aligned} \quad (13)$$

where all constants have been absorbed in $|A_0|^2$.

The result of (13) states that the interlook CCF of speckle complex amplitudes in the subimages centered at azimuth center times T_n and $T_{n'}$ is given by the autocorrelation function of the amplitude weighting function of subreference signals. The CCF of the intensity speckle patterns given by (1) is therefore proportional to the modulus square of (13). It is important to emphasize that the interlook cross-correlation property is dependent only on the subaperture weighting function, and it is independent of the temporal correlation function of (10), provided that the backscattered spatial field is a statistically white random process.

D. Interlook CCF for Rectangular Weighting Function

For a rectangular weighting function

$$\begin{aligned} W\left(\frac{t - T_n}{T}\right) &= \text{rect}\left(\frac{t - T_n}{T}\right) = 1 : -\frac{T}{2} \leq t - T_n \leq \frac{T}{2} \\ &0 : \text{otherwise} \end{aligned} \quad (14)$$

the normalized intensity CCF is readily given by

$$\begin{aligned} C(\Delta T) &\equiv \frac{\langle I(X; T_1)I(X; T_2) \rangle}{\langle I \rangle^2} - 1 \\ &= \left(1 - \frac{\Delta T}{T}\right)^2 \end{aligned} \quad (15)$$

where $\Delta T = |T_1 - T_2| \leq T$ is the center time difference between the look 1 and look 2 subapertures. The two speckle patterns in the subimages are identical when $\Delta T = 0$, and they are, of course, perfectly correlated. As ΔT increases, the overlapping area of subapertures decreases and the speckle patterns start to decorrelate. They decorrelate completely when the center time difference equals ($\Delta T = T$) or ΔT is greater than the integration time, since there is no overlapping area between two subapertures. When these uncorrelated speckle patterns are added on an intensity basis, the speckle fluctuation reduces by the factor of $1/\sqrt{N}$ where N is the number of uncorrelated speckle patterns. This is the basis of speckle reduction by multilook processing.

In spaceborne SARs such as ENVISAT, RADARSAT-1, and JERS-1 SAR, the integration times of a full single look are approximately 0.5–2.0 s, so that the integration times of N -look subimages are in the range between $0.5/N$ and $2.0/N$ s, while the coherence (decorrelation) time of sea surfaces is in the order of 0.05–0.1 s for L-band, and 0.05 s or less for C-band [12]–[18]. It has been suggested that if the interlook speckle patterns were to decorrelate according to the sea surface coherence time (which is much shorter than the integration time of a subaperture), subimages with uncorrelated speckle patterns could be produced through partially overlapped subapertures. Hence, an extra look subimage could be extracted from the raw data of full synthetic aperture length. For example, instead of two subapertures, three partially overlapped subapertures of the same bandwidth could be used to produce three subimages with uncorrelated speckle patterns [19]. However, this cannot be done for the case of Gaussian speckle, since, from the result of (13) and (15), the CCF of intensity speckle patterns is independent of the scene coherence time.

The situation is different for scatterers that give rise to non-Gaussian intensity fluctuations [3], [5], [20], [21]. It can easily be conjectured that the image of an isolated deterministic scattering object such as a corner reflector or transponder must have high degrees of interlook correlation even if the center time difference becomes very large. If the received signal from such a scatterer (elementary scattering object) has temporal fluctuations within the integration time (for example, by randomly varying the return signal from a transponder), the interlook correlation time would be shorter than the integration time. If, therefore, the backscattered field is statistically “non-white” consisting of a few such randomly fluctuating scatterers, then the fluctuations in image intensity obey non-Gaussian statistics, and the interlook CCF becomes dependent on the scene coherence time. Analysis of such situation is given in the previous theoretical study [5], but it is not the purpose of this paper to examine the non-Gaussian speckle. Thus, we restrict the present discussion to the case of Gaussian speckle fluctuations, where the CCF is a function only of the subaperture

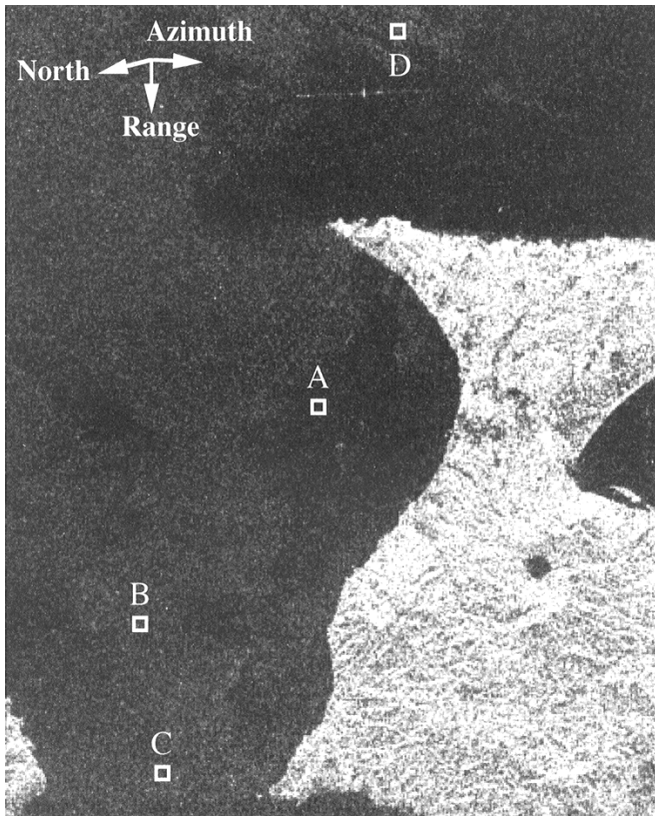


Fig. 1. JERS-1 SAR intensity image of the Tsugaru Strait between the mainland Honshu and Hokkaido, Japan. The size is approximately 68 and 55 km in azimuth and range, respectively. The white boxed areas marked “A”, “B”, “C”, and “D” of size 100×100 pixels are used for the analysis.

weighting function and the interlook time difference, provided that the backscattered field is statistically white.

III. EXPERIMENTAL RESULTS AND DISCUSSION

A. JERS-1 SAR Data

The JERS-1 SAR [22] was in operation from 1992 to 1998 at L-band (wavelength 0.235 m; frequency 1.275 GHz) in HH-polarization with nominal resolution of 6 m (full single-look) in azimuth and 18 m in ground-range directions. It was designed for the global land observation, having the nominal off-nadir angle of 35° to reduce the foreshortening and layover effects, and hence it was considered as being not well suited for oceanic applications. However, under favorable conditions, the JERS-1 SAR data can be used to extract oceanic information [23].

Fig. 1 shows the JERS-1 SAR intensity image of the Tsugaru Strait located between Hokkaido and mainland (Honshu) Japan, and the image center is approximately at $41^\circ 30'N$ and $141^\circ 17'E$, with data acquisition time of 01:23 GMT on June 26, 1997. The ocean currents are strong in the strait flowing from west to east (from “C” to “B” in Fig. 1). According to the Japan Oceanographic Data Center, the maximum current velocity at the area “C” in June is 4.6 knots (2.4 m/s) with mean velocity of 1.1 knots (0.57 m/s). The database of the Japan Weather Association (JWA) show that at the time approximately an hour and half prior to the data acquisition (00:01 GMT), the wind speed was 4.0 m/s from west at the position marked “C” in Fig. 1, and the ocean waves of mean wavelength 0.35 m,

propagating toward the southwest with the period 3.7 s. The image size is approximately 68 and 55 km in azimuth and range directions, respectively. In the image, no clear wave patterns are observed, and the image modulations over the strait appear to be associated with wind and currents. The white boxed areas labeled as “A”, “B”, “C”, and “D” of each size 100×100 pixels are used to test the theory described in Section II. In order to compute the interlook cross-correlation function, the total of nine images of the same area are processed. The bandwidth of the subreference signal is 400 Hz, and the Doppler center frequency is changed from -200 Hz to 200 Hz with interval of 50 Hz. The relation between the Doppler frequency f_D and azimuth time t is given by

$$t = \frac{\lambda R}{2V^2} f_D. \quad (16)$$

For this particular dataset, the relative platform velocity is 7.3 km/s and slant-range distance is 697 km with the incidence angle of 39° at the center of the image of Fig. 1. Then, the azimuth integration time of each subreference signal becomes 0.62 s, and the interlook center time difference is 0.077 s. Both the azimuth and range resolution cells of the subimages are 18 m.

B. RADARSAT-1 SAR Data

The RADARSAT-1 SAR is currently in operation at the radar wavelength of 5.6 cm (5.3 GHz at C-band HH polarization) since its launch in 1995 [24]. Among several beam modes, the Standard Beam 1 is used in this paper, with its nominal incidence angle of 24° , and the nominal azimuth (four-look) and range resolutions of 28 and 25 m, respectively.

Fig. 2 shows the RADARSAT-1 intensity image over the coast of the Yoshino-Kumano National Park and the Kumano Sea (image center: $33^\circ 34'N$, $136^\circ 00'E$) acquired at 21:05 GMT on the 28th of October 1998. The size is approximately 24 km in azimuth and 60 km in range, and the white boxed areas marked as “A”, “B”, “C”, and “D” of each size 100×100 pixels are used for analysis.

The meteorological data from the Japan Weather Association at the time 3 h prior to the RADARSAT pass show the wind speed of 3 m/s from the northwest and significant waveheight of 0.9 m with period of 8 s, propagating from the southeast. A close inspection of the full scene shows the presence of ocean waves in the deep sea in the southeast away from the center of Fig. 2, but no clear wave images are seen in the coastal sea shown in Fig. 2, except some wind and frontal features and several ships with their wake lines. The mean intensity is largest in “A” indicating the presence of some wind, and it is smallest in “D” which is a wind-sheltered area.

In the present analysis, 11 sets of images are processed from the raw data using the subreference signal having the bandwidth of 500 Hz and the center frequencies ranging from -250 Hz to 250 Hz with the center frequency interval of 50 Hz. For the present dataset, the slant-range distance is 983.5 km with the incidence angle of 27° at the center of the image of Fig. 2, and the relative platform velocity is 7.0 km/s. From these parameters, the integration time of each look and interlook time difference are calculated as 0.28 and 0.028 s, respectively, and the azimuth and range resolution cells are 14 and 25 m, respectively.

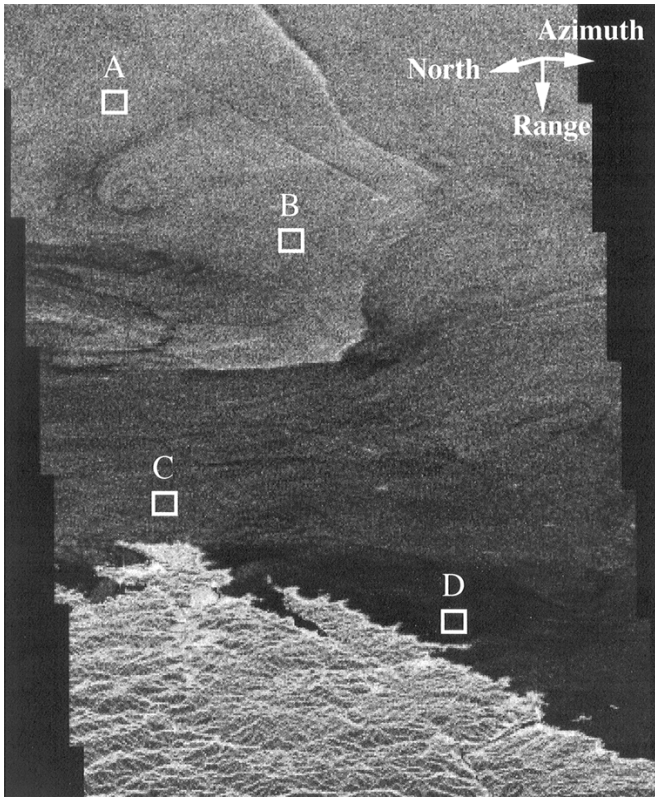


Fig. 2. RADARSAT single-look intensity image of the Kumano Sea, Japan. The size is 24 and 60 km in azimuth and range, respectively. The white boxed areas marked “A”, “B”, “C”, and “D” of size 100 × 100 pixels are used for the analysis.

C. Statistical Analysis of JERS-1 SAR Data

Before taking cross-correlation, the pdf of each area is estimated to ensure that the amplitude and intensity fluctuations constitute a Gaussian speckle pattern. Fig. 3 is the amplitude pdf of the areas “A” in the JERS-1 SAR image of Fig. 1, where the measured pdf represented by the step line is in good agreement with the Rayleigh distribution of the smooth curve. Although not shown in the paper, the intensity pdf of the area “A” closely follows a negative exponential function, and the pdfs of all other areas are also in good agreement with the theoretical distributions.

The data points in Fig. 4 are the CCF values of intensity speckle patterns as a function of center time difference between two subapertures. It can be seen that the measured CCFs in the areas “A”, “B”, and “C” are in excellent agreement with the theoretical result of (15) indicated by the solid line, but the measured CCF in the area “D” is slightly larger than the theoretical curve. Close inspection shows that this is because there are some spatially correlated features in the image. The speckle image of the area “D” is well behaved in terms of the single-point statistics, since the amplitude pdf follows the Rayleigh distribution as in Fig. 5. However, the look 1 and 9 images of the area “D” shown, respectively, in the left and center images of the upper row of Fig. 6 are not statistically homogeneous and the spatial features seem to retain some correlation between look 1 and 9. The top-right image shows the coherence image, i.e., a map of correlation values, estimated by using 10 × 10 moving windows. The image is thresholded such that the bright pixels

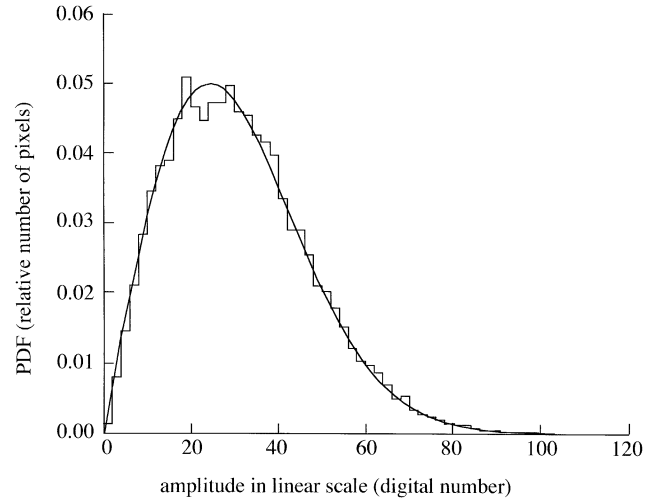


Fig. 3. PDF of speckle amplitude corresponding to the area “A” in the JERS-1 SAR image shown in Fig. 1. The vertical axis is the relative number of pixels, and the horizontal axis is the amplitude in digital number. The measured amplitude pdf represented by the step line closely follows the Rayleigh distribution of the smooth curve.

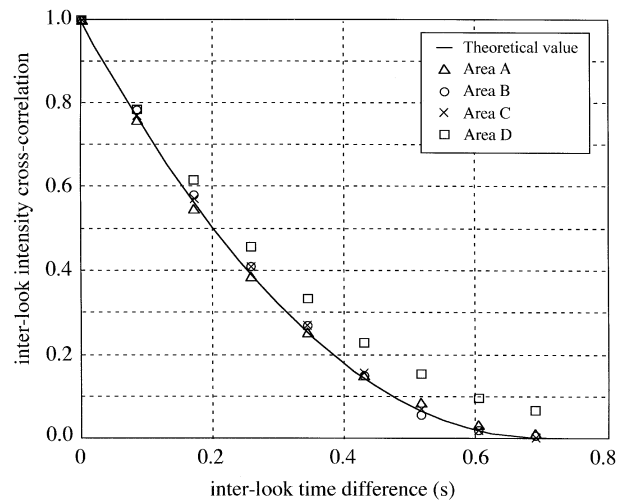


Fig. 4. Interlook cross-correlation function of the area “A”, “B”, “C”, and “D” in the JERS-1 SAR image shown in Fig. 1 as a function of the center time difference. The solid line is the theoretical curve based on (15).

correspond to the degree of coherence larger than 0.35. A certain number of pixels with high degrees of coherence explain the discrepancy of the area “D” in Fig. 4. Note that large-scale correlated features visible in the left and center images in the upper row of Fig. 6 are not captured in the coherence image, because of the small size of the moving windows.

The look 1 and 9 images of the area “A” shown in the lower row of Fig. 6 appear to be statistically uniform with little correlation between looks. The coherence image on the right also indicates that there are very small number of pixels with the degrees of coherence above 0.35. Thus, the correlated spatial features are the main reason why the degree of interlook cross-correlation in the area “D” is higher than the theoretical result of (15).

There are no simultaneous sea truth data on the scene coherence time, but in general the coherence time is approximately 0.1 s or less as mentioned in Section II. Therefore, if the scene

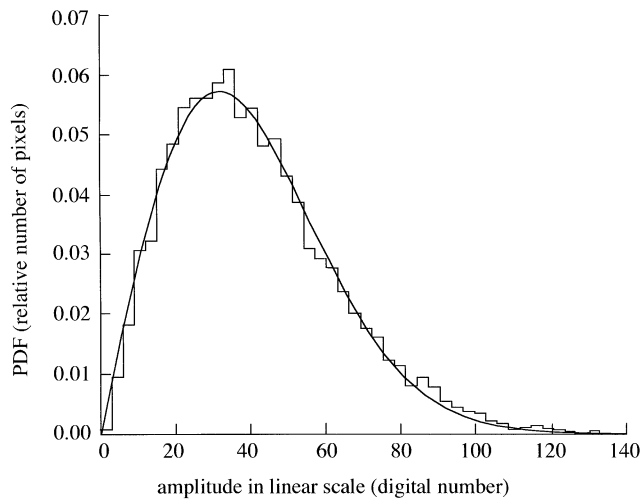


Fig. 5. PDF of speckle amplitude corresponding to the area "D" in the JERS-1 SAR image shown in Fig. 1. The vertical axis is the relative number of pixels, and the horizontal axis is the amplitude in digital number. The measured amplitude pdf represented by the step line closely follows the Rayleigh distribution of the smooth curve.

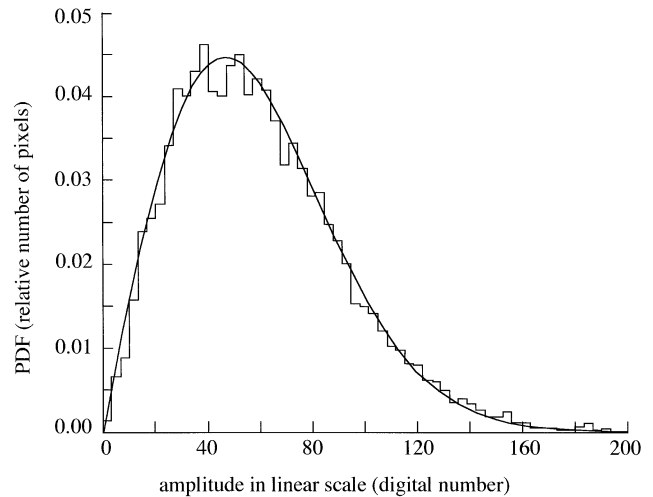


Fig. 7. PDF of speckle amplitude of the area "A" in the RADARSAT-1 image shown in Fig. 2. The vertical axis is the relative number of pixels, and the horizontal axis is the amplitude in digital number. The measured amplitude pdf represented by the step line closely follows the Rayleigh distribution of the smooth curve.

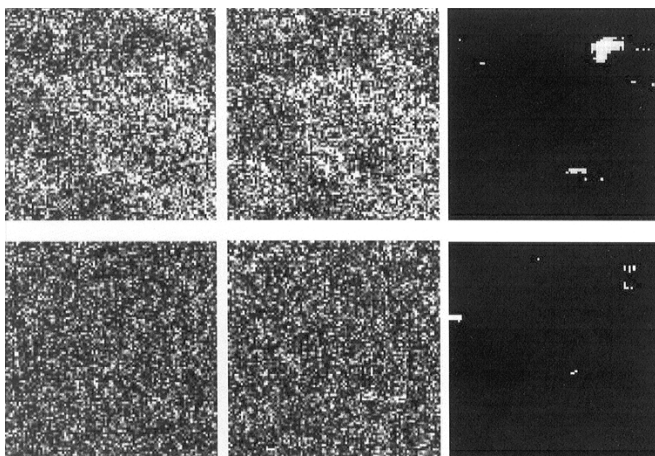


Fig. 6. Left and center images in the upper row are, respectively, the look 1 and 9 images of the area "D" in Fig. 1, and those in the lower row are the look 1 and 9 images of the area "A", respectively. The right images are the corresponding coherence images produced by cross-correlating the look 1 and 9 images with moving windows of size 10×10 pixels and thresholding by the correlation value of 0.35.

coherence time were to enter the interlook cross-correlation function, then the interlook speckle patterns should have decorrelated at time lags of similar order, and the measured CCF in Fig. 4 should have had shorter correlation times than the theoretical solid curve. The result shown in Fig. 4 is an evidence that this is not the case, and the interlook CCF of speckle patterns is independent of the random temporal fluctuation of the backscattered field as predicted by (13) and (15), provided that the backscattered field is modeled as a statistically white random process.

D. Statistical Analysis of RADARSAT-1 Data

Fig. 7 is the amplitude pdf of the area "A" in the RADARSAT-1 image shown in Fig. 2. Again, good agreement can be seen between the measured pdf and Rayleigh

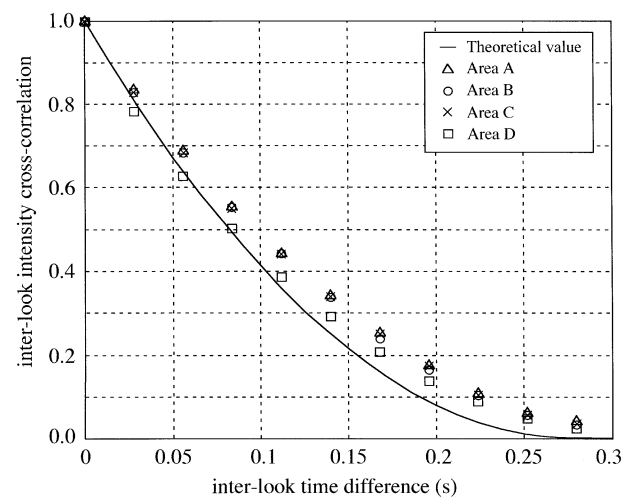


Fig. 8. Interlook cross-correlation function of the area "A", "B", "C", and "D" in the RADARSAT-1 image shown Fig. 1 as a function of the center time difference. The solid line is the theoretical curve based on (15).

distribution. Good agreement on the amplitude and intensity pdfs is also obtained in the images of other areas.

Fig. 8 is the interlook cross-correlation function of the RADARSAT-1 test images as a function of center time difference. The measured CCF values tend to overestimate the theoretical curve mainly because of spatially correlated features (although the features are not as clear as those in Fig. 6). This spatial correlation can be seen in Fig. 9, where the left and center images are the look 1 and 11 images of the area "D" in Fig. 2, and the right is the coherence image estimated by the same way as in Fig. 6. Again, there exist some pixels of high correlation, explaining the discrepancy between the theory and experimental results seen in Fig. 8.

The CCF measurements given by Fig. 8 provide a further support to the theoretical result of (15) on the cross-correlation function of speckle intensity in the images produced by partially overlapped subapertures.

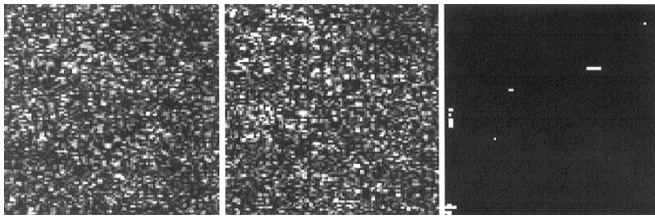


Fig. 9. Left and center images are, respectively, the look 1 and 11 images of the area "D" in Fig. 2. The right image is the coherence image produced by cross-correlating the look 1 and 11 images with moving windows of size 10×10 pixels, and thresholding by the correlation value of 0.35.

IV. CONCLUSION

In the present paper, a general integral expression is derived for the intensity CCF of interlook speckle patterns in the subimages processed with partially overlapped subapertures, and a simple analytical expression is derived for a rectangular subaperture weighting function. The results show that, for statistically white (spatially homogeneous noncorrelated) backscattered fields which give rise to the classical Gaussian speckle, the CCF depends only on the amplitude weighting function and center time difference of subapertures; and that it is independent of the temporal correlation properties of the backscattered fields. This theoretical conclusion is supported by the JERS-1 L-band and RADARSAT-1 C-band SAR images over the coastal waters of Japan.

ACKNOWLEDGMENT

The JERS-1 SAR raw data were provided by the Japan Aerospace Exploration Agency (JAXA). The Canadian Space Agency is the owner of the RADARSAT-1 data used in this paper. The RADARSAT raw data were purchased by the Mitsubishi Heavy Industries Ltd., and processed at Kochi University of Technology. The meteorological data of the Tsugaru Strait and Kumano Sea were provided by the Japan Weather Association, and the current data of the Tsugaru Strait were due to the Japan Oceanographic Data Center.

REFERENCES

- [1] J. W. Goodman, "Statistical properties of laser speckle patterns," in *Laser Speckle and Related Phenomena*, J.C. Dainty, Ed. Berlin, Germany: Springer-Verlag, 1975, pp. 19–26.
- [2] J. S. Lee and I. Jurkevich, "Speckle filtering of synthetic aperture radar imagery: A review," *Remote Sens. Rev.*, vol. 8, pp. 313–340, 1994.
- [3] C. Oliver and S. Quegan, *Understanding Synthetic Aperture Radar Images*. London, U.K.: Artech House, 1998.
- [4] L. J. Porcello, N. G. Massey, R. B. Innes, and J. M. Marks, "Speckle reduction in synthetic aperture radar," *J. Opt. Soc. Amer.*, vol. 66, pp. 1305–1311, 1976.
- [5] K. Ouchi and R. E. Burge, "Speckle cross-correlation function in multilook SAR images of moving discrete scatterers," *Int. J. Remote Sens.*, vol. 12, pp. 1933–1946, 1991.
- [6] K. Ouchi, S. Tamaki, H. Yaguchi, and M. Iehara, "Ship detection based on coherence image derived from cross-correlation of multilook SAR images," *IEEE Geosci. Remote Sens. Lett.*, vol. 1, pp. 184–187, Jan. 2004.
- [7] A. Papoulis, *Probability, Random Variables, and Stochastic Processes*, 3rd ed. New York: McGraw-Hill, 1991, pp. 214–221.
- [8] H. Goldstein, "The fluctuations of clutter echos," in *Propagation of Short Radio Waves*, ser. 13, D.E. Kerr, Ed. New York: McGraw-Hill, 1951, pp. 554–554.
- [9] A. J. F. Siegert, "On the fluctuations in signals returned by many independently moving scatterers," MIT Radiation Lab., Cambridge, MA, Tech. Rep., 1943.

- [10] R. K. Raney, "SAR response to partially coherent phenomena," *IEEE Trans. Antennas Propagat.*, vol. AP-28, pp. 777–787, 1980.
- [11] A. M. Smith, "A new approach to range-Doppler SAR processing," *Int. J. Remote. Sens.*, vol. 12, pp. 235–251, 1991.
- [12] W. R. Alpers and C. Brüning, "On the relative importance of motion-related contributions to the SAR imaging mechanism of ocean surface waves," *IEEE Trans. Geosci. Remote. Sens.*, vol. GE-24, pp. 873–885, 1986.
- [13] R. E. Crande, "Estimating ocean coherence time using dual-baseline interferometric synthetic aperture radar," *IEEE Trans. Geosci. Remote. Sens.*, vol. 32, no. 6, pp. 846–854, Jun. 1994.
- [14] S. J. Frasier and A. J. Camps, "Dual-beam interferometry for ocean surface current vector mapping," *IEEE Trans. Geosci. Remote. Sens.*, vol. 39, no. 2, pp. 401–414, Feb. 2001.
- [15] D. P. Kasilingham and O. H. Shemdin, "Theory for synthetic aperture radar imaging of the ocean surface: With application to the tower ocean wave and radar dependence experiment of focus, resolution and wave height spectra," *J. Geophys. Res.*, vol. 93, no. C11, pp. 13 837–13 848, 1988.
- [16] W. J. Plant and W. C. Keller, "Evidence of Bragg scattering in microwave doppler spectra of sea return," *J. Geophys. Res.*, vol. 95, no. C9, pp. 16 299–16 310, 1990.
- [17] L. Shemer and M. Marom, "Estimates of ocean coherence time by an interferometric SAR," *Int. J. Remote. Sens.*, vol. 14, no. 16, pp. 3021–3029, 1993.
- [18] M. J. Tucker, "The decorrelation time of microwave radar echoes from the sea surface," *Int. J. Remote. Sens.*, vol. 6, pp. 1075–1089, 1985.
- [19] R. K. Raney and P. W. Vachon, "Synthetic aperture radar imaging of ocean waves from an airborne platform: Focus and tracking issues," *J. Geophys. Res.*, vol. 93, no. C10, pp. 12 475–12 486, 1988.
- [20] C. J. Oliver, "The representation of radar sea clutter," *Proc. Int. Elect. Eng., F*, vol. 135, pp. 497–500.
- [21] K. Ouchi and R. A. Cordey, "Statistical analysis of azimuth streaks observed in digitally processed CASSIE imagery of sea surface," *IEEE Trans. Geosci. Remote. Sens.*, vol. 29, no. 5, pp. 727–735, Sep. 1991.
- [22] Y. Nemoto, H. Nishio, M. Ono, H. Mizutamari, K. Nishioka, and K. Tanaka, "Japanese earth resources satellite-1 synthetic aperture radar," *Proc. IEEE*, vol. 79, no. 6, pp. 800–809, Jun. 1991.
- [23] K. Ouchi and H. Mitsuyasu, "Determination of ocean wave propagation direction by split-look processing using JERS-1 SAR data," *IEEE Trans. Geosci. Remote. Sens.*, vol. 37, no. 2, pp. 849–855, Mar. 1999.
- [24] R. K. Raney, A. P. Luscombe, E. J. Langham, and A. Ahmed, "RADARSAT," *Proc. IEEE*, vol. 79, no. 6, pp. 839–849, Jun. 1991.



Kazuo Ouchi (M'85–SM'99) received the B.Sc. degree in physics from the College of Science and Technology, Nihon University, Tokyo, Japan, in 1971, the B.Sc. degree in physics from Southampton University, Southampton, U.K., in 1976, the M.Sc. and D.I.C. degrees in applied optics in 1977, and the Ph.D. degree in 1981 from the Imperial College of Science, Technology and Medicine, University of London, London, U.K.

From 1980 to 1982, he was a Research Assistant in the Blackett Laboratory, Physics Department, Imperial College, and also a consultant for the Oxford Computer Services Ltd., Oxford, U.K. From 1982 to 1992, he was a Research Associate in the Wheatstone Laboratory, King's College, University of London. He returned to the Blackett Laboratory, Imperial College from 1992 to 1996 as a Research Fellow, before becoming a Professor in the Department of Environmental Studies, Hiroshima Institute of Technology, Japan from 1996 to 1999. He is currently a Professor in the Department of Environmental Systems Engineering, Kochi University of Technology, Kochi, Japan. His research subjects include SAR/InSAR/PoSAR systems and applications to land and ocean, EM scattering, speckle statistics, and microwave/optical remote sensing.



Haipeng Wang (S'04) received the B.S. and M.S. degrees in mechanical and electronic engineering from Harbin Institute of Technology, Harbin, China, in 2001 and 2003, respectively. He is currently pursuing the Ph.D. degree in radar remote sensing at the Graduate School of Engineering, Kochi University of Technology, Japan.